Excited-State Proton Transfer in 7-Hydroxy-4-methylcoumarin along a Hydrogen-Bonded Water Wire

Ivelina Georgieva and Natasha Trendafilova*

Institute of General and Inorganic Chemistry, Bulgarian Academy of Sciences, Sofia, Bulgaria

Adélia J. A. Aquino and Hans Lischka*

Institute for Theoretical Chemistry, Währingerstrasse 17, University of Vienna, A-1090 Vienna, Austria

Received: September 22, 2006; In Final Form: October 23, 2006

TDDFT, RI-CC2, and CIS calculations have been performed for the nondissociative excited-state proton transfer (ESPT) in the S_1 state of 7-hydroxy-4-methylcoumarin (7H4MC) along a H-bonded water wire of three water molecules bridging the proton donor (OH) and the proton acceptor (C=O) groups (7H4MC·$(H_2O)_3$). The observed structural reorganization in the water-wire cluster is interpreted as a proton-transfer (PT) reaction along the H_2O solvent wire. The shift of electron density within the organic chromophore 7H4MC due to the optical excitation appears to be the driving force for ESPT. All the methods used show that the reaction path occurs in the $^1\pi\pi^*$ state, and no crossing with a Rydberg-type $^1\pi\sigma^*$ state is found. TDDFT and RI-CC2 calculations predict an exoergic reaction of the excited-state enol-to-keto transformation. The S_1 potential energy curve reveals well-defined C_s minima of enol- and keto-clusters, separated by a single barrier with a height of 17−20 kcal/mol. After surmounting this barrier, spontaneous PT along the water wire is observed, leading without any further barrier to the keto structure. The TDDFT and RI-CC2 methods appear to be reliable approaches to describe the energy surfaces of ESPT. The CIS method predicts an endoergic ESPT reaction and an energy barrier, which is too high.

I. Introduction

The photoinduced proton and hydrogen atom transfer (PT/HT) reactions are of great importance in photochemistry and photobiology. The amphoteric bifunctional molecules whose functions become more acidic or basic upon electronic excitation undergo proton transfer via H-bonded vicinal groups,[1] concerted biprotonic transfer within a doubly H-bonded dimer,[2] coupled proton and electron transfer,[3] intermolecular double PT with solvent molecules[4−6] and PT or HT along a wire of solvent molecules between two spatially separated functional groups within the same molecule.[3,7−10]

7-Hydroxy-4-methylcoumarin (7H4MC) is of special interest since (1) there is spectroscopic evidence for excited-state enol-to-keto tautomerization in aqueous solution and (2) its enol form possesses a proton donor group (O−H) at a large distance to a proton acceptor group (C=O) so that direct intramolecular PT is not possible (Figure 1a). Electronic excitation to the S_1 state strongly modifies the acid−base properties of 7H4MC, rendering the hydroxyl group more acid, S_0 ($pK_a \sim 7.7$) and S_1 ($pK_a \sim 0.45$).[11] 7H4MC has been widely investigated both from experimental and theoretical viewpoints[4,11−18] because of its remarkable photophysical properties, utilized in diverse areas such as fluorescent indicators and laser dye colorants, nonlinear optical chromophores, and excellent probes for studying solvation dynamics in homogeneous solutions and organized media.[12,19] Hydroxycoumarins (HCs) are well-known natural products,[20] which have been described as enzyme inhibitors, as agents with anticoagulant,[21] spasmolytic,[22] and anticancer activity,[23] as sun protection agents,[24] and as pesticides.[25]

In the excited state, 7H4MC shows four possible fluorescent species, depending on solvent and pH: enol (**E***), anion (**A***), cation (**C***), and a long-wavelength emitting keto-tautomeric form (**K***), whereas in the ground state only the **E**, **A**, and **C** forms exist. Therefore, the **K*** form is an excited-state reaction product, which arises from the **E*** form through proton transfer from the acidic (OH) to the basic (C=O) group in the excited state. The prototropic transformations of 7H4MC have already been investigated experimentally in aqueous or aqueous−alcoholic solutions by means of steady-state[4,14−16,26,27] or time-resolved fluorometry.[13,28] Two different mechanisms of photoexcited tautomerization processes were discussed in the literature—"dissociative" two-step pathways via the **A*** or **C*** species[4,14] and a nondissociative one-step reaction of **E*** ↔ **K*** tautomer conversion.[15,16] The spectroscopic and kinetic measurements in hydroxylic solvents suggested that a concerted bifunctional proton transfer through water molecules is the most probable process.[15,16] The presence of water favors the excited-state tautomerization: with an increase of the water content in water−alcohol mixtures the **K*** band grows at the expense of the **E*** band.

7-Hydroxyquinoline (7HQ) has also been studied intensively as a model for nondissociative proton transfer through a wire of solvent molecules.[7,8,10,29−37] In 7HQ·$(NH_3)_3$ clusters, $S_0 \rightarrow S_1$ photoexcitation of 7HQ triggered hydrogen transfer along the ammonia chain. In contrast, supersonic jet cooled 7HQ·$(H_2O)_n$ water-wire clusters with $n = 1−6$ have not shown evidence of hydrogen transfer along the water wire.[30−33] Electronic structure calculations on the ground and excited states of 7HQ·$(NH_3)_3$ have shown that the S_1 enol → keto tautomerization arises from a curve crossing of the $^1\pi\pi^*$ with an

* Corresponding author. E-mail: hans.lischka@univie.ac.at (H.L.); ntrend@svr.igic.bas.bg (N.T.).
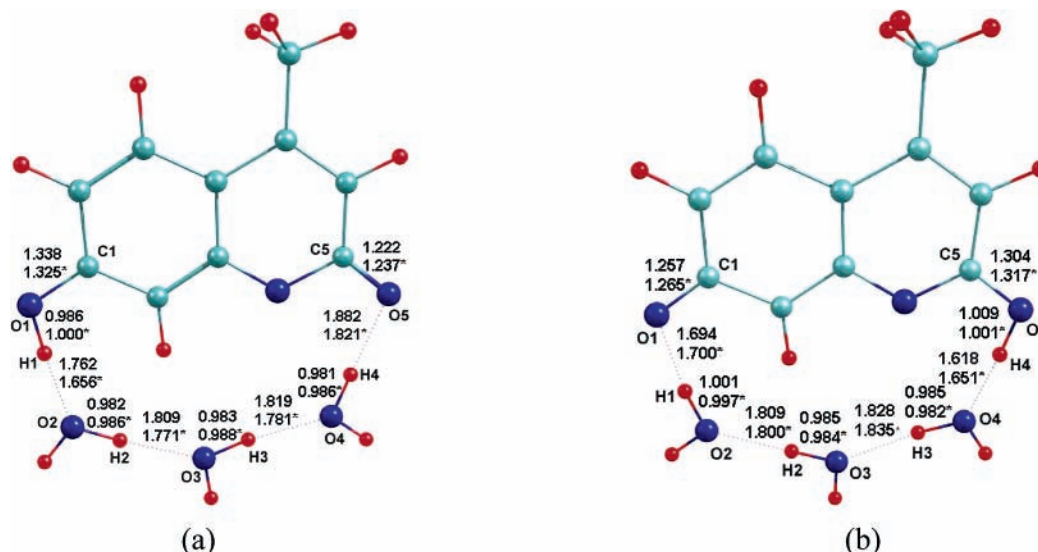
Figure 1. Optimized structures of **E**·(H$_2$O)$_3$ (a) and **K**·(H$_2$O)$_3$ (b) in S$_0$ and S$_1$^{1}($\pi\pi^*$) states at the DFT/SVPD level. S$_1$ bond lengths are denoted by an asterisk.

optically dark $^1\pi\sigma^*$ state.[10] The importance of the $^1\pi\pi^*/^1\pi\sigma^*$ crossings for the hydrogen-transfer processes has been pointed out originally by Sobolewski and co-workers.[38−41]

7H4MC, with its OH proton donor group and a C=O oxygen proton acceptor atom, appears to be a suitable model for the theoretical study of the excited-state enol → keto tautomerization in aqueous solution via a nondissociative mechanism. The 7H4MC·(H$_2$O)$_3$ cluster model used here with three water-wire molecules is different from 7HQ·(NH$_3$)$_3$ in relation to the type of the acceptor site (O/N) and the type of solvent wire (H$_2$O/ NH$_3$).

The goal of our work is to investigate theoretically the reaction path of the nondissociative proton-transfer reaction of 7-hydroxy-4-methylcoumarin in the excited-state using the 7H4MC·(H$_2$O)$_3$ cluster model. Due to the size of the 7H4MC-water cluster, time-dependent density functional theory (TDDFT)[42−44] has been selected as a computationally efficient method for excited-state calculations. It has the potential to give results of accuracy comparable to the CASPT2 method and is significantly better than CIS.[45] The applicability of TDDFT for calculation of potential energy profiles of ESPT along a H-bonded solvent wire is much less known. To avoid possible artifacts of TDDFT, the approximate coupled cluster singles and doubles method (CC2)[46] augmented by the resolution-of-the-identity (RI) method[47] has been used to assess the reliability of TDDFT in the present study. This procedure has already been successfully followed in previous ESIPT studies[48] and in investigations on the excited-state properties of 7H4MC.[18] The configuration interaction method with singles (CIS) has been mainly used for comparison with the aforementioned calculations on the 7HQ·(NH$_3$)$_3$ complex. To explore the possibility of excited-state crossings in the course of the PT process, the energy profiles of the low-lying $\pi\pi^*$, $n\pi^*$, and $\pi\sigma^*$ states have also been calculated. Natural population analysis in the excited state is performed to decide whether proton or hydrogen atom transfer occurs during the enol* → keto* tautomerization.

II. Computational Procedures

The TURBOMOLE program package[49] has been used for the DFT, TDDFT,[42−44] RI-CC2,[47,50] and CIS calculations. Analytic TDDFT gradients have been calculated using the variational TDDFT formulation of Furche and Ahlrichs.[42] Previous studies

on the applicability of the TDDFT method to ESIPT processes has shown that the B3LYP[51] functional seems to be reliable because of the good agreement with RI-CC2 results.[48] The RI approximation was used in CC2 calculations as described in refs 46 and 47 with excited-state analytic gradients developed by Köhn and Hättig.[50] The RI basis set used in the RI-CC2 calculations is described in ref 52. For comparison, the CIS method was also applied.

For the construction of the reaction path, the coordinate-driven reaction path approach has been adopted, i.e., for a given value of R(O$_1$−H$_1$) (Figure 1a) all remaining coordinates have been optimized for the S$_1$($\pi\pi^*$) state. The O$_1$−H$_1$ coordinate was increased stepwise by a 0.1 Å increment. The geometry optimizations in the ground and in the S$_1$($^1\pi\pi^*$) states have been performed using DFT/TDDFT together with the SV(P)[53] (in C_s and C_1 symmetry) and SVPD (SVP+diffuse functions)[53] basis sets (in C_s symmetry). Diffuse functions for the C, O, and H atoms (one s and one p set) were added to the standard SVP basis set (C, O [3s2p1d], H [2s1p]) in order to improve the description of the negatively charged molecular regions. The exponents of the additional basis functions were obtained by dividing the smallest respective exponent of the SVP basis sets by a factor of 3, giving for C $\alpha_s = 0.0436$ and $\alpha_p = 0.0509$, for O $\alpha_s = 0.0851$ and $\alpha_p = 0.0921$, and for H $\alpha_s = 0.0406$ and $\alpha_p = 0.2667$. The final contracted basis set of SVPD is [4s3p1d] for the O and C atoms and [3s2p] for the H atom. Further, single-point calculations along the reaction path have been performed with the TDDFT/SVPDD (SVPD + one additional diffuse s function on the heavy atoms and on the hydrogen atoms, C $\alpha_s = 0.01453$, O $\alpha_s = 0.02837$, H $\alpha_s = 0.01353$), CC2/SV(P), CC2/SVPD, and CIS/SVPD methods. Diffuse basis functions are of crucial importance for the description of the excited-state surface involved in the hydrogen atom transfer reaction, as was shown for the enol−keto tautomerization of 7HQ·(NH$_3$)$_3$.[10] For comparison, in the latter work diffuse functions with exponents of $\alpha_s = 0.0119$ and $\alpha_p = 0.0374$ have been added to the four hydrogen atoms of the ammonia wire.

Intermolecular interaction energies were computed in the ground and in the excited states using the counterpoise (CP) procedure to compensate for the basis set superposition error (BSSE).[54−57] Solvent effects on the ground-state and on the

ESPT in 7H4MC along a Hydrogen-Bonded Water Wire

J. Phys. Chem. A, Vol. 111, No. 1, 2007 **129**

TABLE 1: Relative Energies, kcal/mol, Calculated at the TDDFT/SVPD, RI-CC2/SVP, and CIS/SVPD Levels

symmetry	species	S_0 (DFT/CC2)	$S_1(\pi\pi^*)$ (TDDFT) S_0 optimized geom	$S_1(\pi\pi^*)$ (TDDFT/CC2/CIS) S_1 optimized geom
C_s	**E**·$(H_2O)_3$	$0.0/0.0^a$	0.0^b	$0.0/0.0/0.0^c$
C_s	**K**·$(H_2O)_3$	18.7/20.8	−0.6	−4.6/−7.4/5.7
C_1	**E**·$(H_2O)_3$	−0.9	−0.9	−1.6
C_1	**K**·$(H_2O)_3$	17.8	−1.6	−5.7
C_s	**E**·$(H_2O)_3(H_2O)_2$	0.0^d	0.0^e	0.0^f
C_s	**K**·$(H_2O)_3(H_2O)_2$	$18.0 (15.0)^g$	$-1.3 (-2.8)^g$	$-5.0 (-3.7)^h$

a Total energies:−839.887 014/−837.902 006 au. *b* Total energy: −839.743 391 au. *c* Total energies: −839.748 506/−837.891 535/−835.299 029 au. *d* Total energy: −992.590 533 au. *e* Total energy: −992.445 787 au. *f* Total energy: −992.451 271 au. *g* PCM calculation with the S_0-optimized geometry in the gas phase. *h* PCM calculation with the S_1-optimized geometry in the gas phase.

excited-state properties of 7H4MC were examined using the polarizable continuum model (PCM) of Tomasi et al.[58−60] as implemented in the GAUSSIAN03 package.[61] To describe the specific interactions of 7H4MC with the solvent, two cluster models are considered, 7H4MC·$(H_2O)_3$ and 7H4MC·$(H_2O)_3$-$(H_2O)_2$. The 7H4MC·$(H_2O)_3(H_2O)_2$ cluster contains in addition one water molecule bonded to the C=O group ($H_w\cdots O=C$) and another one bonded to the COH group ($H_w\cdots O(H)C$). The solvent effect on the vertical excitation energy of 7H4MC·$(H_2O)_3(H_2O)_2$ tautomers was computed using the optimized ground-state structures in the gas phase. The solvent effect on the fluorescence properties was calculated for the optimized excited-state structures. The electron density differences of the ground and the excited states of 7H4MC species have been computed with the CIS method and the SVP basis set using the GAUSSIAN03 program. The CIS/SVP method has been used for a natural population analysis in the ground and in the excited states.[62]

III. Results and Discussion

III.A. Energetic Properties of the Tautomerization Process. The photophysical properties, the energetics of **E** and **K** forms, their interactions with two and four water molecules, and bulk solvation effects have been investigated in our previous study.[18] In the $^1\pi\pi^*$ state, the **K** structure is more stable than the **E** structure, both in the gas phase and in the aqueous solution (PCM) by 3.5 and 2.7 kcal/mol, respectively.[18] In the present study we concentrate on the excited-state tautomerization process in 7H4MC. The ESPT is modeled along the three H-bonded water molecules bridging the proton donor $H_1(O_1)$ and the proton acceptor $O_5(=C_5)$ groups of 7H4MC, Figure 1a. The determination of the equilibrium structures of **E**- and **K**-water clusters and their relative stabilities provides first information on how the molecular frame readjusts during the proton transfer. The **E**·$(H_2O)_3$ and the **K**·$(H_2O)_3$ clusters (Figure 1a,b, respectively) were optimized in S_0 and S_1 ($\pi\pi^*$) states in C_s and C_1 symmetries using TDDFT/B3LYP with SV(P) and SVPD basis sets. Both basis sets gave similar results for the geometry parameters and the relative energies. In the following, the discussion is carried out on the structural and energetic data obtained at the TDDFT/SVPD level. In Table 1, the relative energy of the **K**·$(H_2O)_3$ cluster (calculated with respect to the **E**·$(H_2O)_3$ cluster) is given for the S_0 and S_1 states. In the S_0 state, the **E**·$(H_2O)_3$ cluster is more stable than the **K**·$(H_2O)_3$ cluster by 18.7 kcal/mol (B3LYP) and hence no enol → keto proton transfer occurs in 7H4MC.[14] In the S_1 state (using the DFT ground-state geometries) the **K**·$(H_2O)_3$ structure is more stable by 0.6 kcal/mol. After excited-state optimization the **K**·$(H_2O)_3$ stability increases to 4.6 kcal/mol. The RI-CC2 method gives analogous trends and thus supports the reliability of the DFT results. As distinct from TDDFT and CC2 methods, the CIS calculations predict the **E**·$(H_2O)_3$ cluster as the more stable

tautomer in the excited state. The structures in C_1 symmetry showed lower energies (by ~1 kcal/mol) in comparison with the corresponding C_s structures. Since the relative energies of the **E** and **K** cluster tautomers obtained with C_1 or C_s calculations are very similar, the C_s calculations are predominantly used for reasons of computational efficiency. The effect of the out-of-plane distortions is discussed below.

The solvent effects were considered through augmenting 7H4MC·$(H_2O)_3$ by two additional water molecules (specific solvation): one attached to the enol group and the other one to the carbonyl group and by using additionally the PCM method (global solvation). As can be seen from Table 1, both cluster models, 7H4MC·$(H_2O)_3$ and 7H4MC·$(H_2O)_3(H_2O)_2$, give close relative energies with differences up to 1 kcal/mol in S_0 and S_1 states. The PCM model produces a stabilization of the **K**·$(H_2O)_3$-$(H_2O)_2$ cluster in the S_0 state and a slight destabilization of the **K**·$(H_2O)_3(H_2O)_2$ in the S_1 state. In total, the **K** form is energetically favored in the $S_1(\pi\pi^*)$ state, demonstrating the energetic feasibility of proton transfer from the **E*** to the **K*** form.

III.B. Spectroscopic Data of the 7H4MC·$(H_2O)_n$ Tautomers. Calculated vertical excitation, emission, and adiabatic energies of the 7H4MC·$(H_2O)_3$ and 7H4MC·$(H_2O)_3(H_2O)_2$ tautomers are given in Table 2 for the gas phase and in solution in comparison to available experimental spectroscopic data of 7H4MC in aqueous solution (absorption and fluorescence). The lowest excited state for the tautomers studied is the $2^1A'(\pi\pi^*)$ in the gas phase and in aqueous solution. As it can be seen from Table 2, the vertical excitation energy of the enol 7H4MC·$(H_2O)_3(H_2O)_2$ cluster is close to the experimental absorption data in solution within 0.15 eV. It should be noted that the comparison of the experimental excitation energy in solution (3.86 eV) and the calculated one for isolated 7H4MC (4.13 eV)[18] indicates a negative solvent shift. In agreement with this finding the calculated solvent shifts of 7H4MC·$(H_2O)_3$, 7H4MC·$(H_2O)_3$-$(H_2O)_2$, and 7H4MC·$(H_2O)_3(H_2O)_2$ in solution with respect to the isolated 7H4MC are also negative. The continuum model only slightly increases the vertical excitation energy, indicating that both water cluster models reliably reproduce the solute−solvent interactions. Experimental absorption data for the **K** form are not available because of its instability.

The vertical fluorescence energies of **E**-water clusters amount to 3.63, 3.64, and 3.71 eV, depending on the cluster type and the environment (see Table 2), and are about 0.5 eV larger than the experimental value of 3.18 eV. The computed gas-phase fluorescence energy of the isolated **E** form is 3.73 eV,[18] and the major source for the discrepancy to experiment was already discussed there. Both **K**-water clusters show larger fluorescence energies (2.38, 2.41 eV) than that of the isolated **K** form (2.28 eV)[18] and thus tend toward experiment (2.61 eV). Furthermore, due to the positive solvent shift obtained with the PCM model,

TABLE 2: TDDFT/SVPD Vertical Excitation (abs), Emission (fl), and Adiabatic (m−m) Energies, eV, of the Singlet Excited States of Water−Wire 7H4MC Tautomer Clusters (ν_{st}, Stokes Shift)[a,b]

geometry	state	abs	fl	m−m	ν_{st}
$E \cdot (H_2O)_3$	2^1A $(\pi\pi^*)$	3.91/(0.285)	3.63/(0.266)	3.77	0.28
	3^1A $(\pi\pi^*)$	4.32 (0.003)			
	1^1A $(n\pi^*)$	4.92			
$K \cdot (H_2O)_3$	2^1A $(\pi\pi^*)$	3.07 (0.266)	2.38/(0.107)	2.76	0.69
	3^1A $(\pi\pi^*)$	4.15 (0.056)			
	1^1A $(n\pi^*)$	3.42			
$E \cdot (H_2O)_3(H_2O)_2$	2^1A $(\pi\pi^*)$	3.94 (0.312)	3.64 (0.286)	3.79	0.30
		4.01^w, $\mathbf{3.86}^{[15,16]}$ (0.337)	3.71^w, $\mathbf{3.18}^{[15,16]}$ (0.313)		
	3^1A $(\pi\pi^*)$	4.31 (0.005)			
		4.42^w (0.003)			
	1^1A $(n\pi^*)$	5.11			
		5.06^w			
$K \cdot (H_2O)_3(H_2O)_2$	2^1A $(\pi\pi^*)$	3.10 (0.243)	2.41 (0.114)	2.79	0.69
		3.24^w (0.281)	2.69^w, $\mathbf{2.61}^{[15,16]}$ (0.134)		
	3^1A $(\pi\pi^*)$	4.07 (0.066)			
		4.24^w (0.050)			
	1^1A $(n\pi^*)$	3.66			
		3.89^w			

[a] Oscillator strengths of the $\pi\pi^*$ state are given in parentheses. Oscillator strengths for $n\pi^*$ transitions are less than 10^{-3}. [b] Experimental values in solution are presented in italics. Superscript w indicates PCM calculations (water solvent) with optimized structures in the gas phase.

the calculated fluorescence energy of the **K** cluster (2.69 eV) is in very good agreement with experiment in aqueous solution.

Since the addition of two water molecules to the 7H4MC·$(H_2O)_3$ clusters showed only a relatively small influence on the solvation energies, we continued our studies on the proton-transfer process using the simpler 7H4MC·$(H_2O)_3$ model.

III.C. Calculated Equilibrium 7H4MC·$(H_2O)_3$ Structures and Hydrogen Bond Energies. A survey of the calculated structural parameters of **E**-water and **K**-water chains is presented in Figure 1. Comparing with the isolated **E** structure, the O_1−H_1 bond of the **E**·$(H_2O)_3$ cluster is stretched by 0.02 Å in S_0 and by 0.03 Å in the S_1 state; see Table 1S of the Supporting Information. Upon excitation of **E**·$(H_2O)_3$, the $(O_1)H_1 \cdots O_{2w1}$ bond is shortened by ∼0.11 Å and the $C_5{=}O_5$ bond is elongated by 0.015 Å. The elongation of the O_1−H_1 bond and the shortening of the $(O_1)H_1 \cdots O_{2w1}$ bond in **E***·$(H_2O)_3$ facilitate the deprotonation process and the proton transfer to the solvent molecule. The $C_5{=}O_5$ bond elongation produces an increase of the proton affinity of the O_5 atom. It was found that upon excitation the formation energy of **E***·$(H_2O)_3$ with respect to three isolated water molecules becomes more negative by 3.5 kcal/mol, which is in agreement with the contraction of H-bond lengths, Table 2S of the Supporting Information. Moreover, in the S_1 state, the calculated interaction energy of the $H_1 \cdots O_{2w1}$ and $H_{4w3} \cdots O_5$ bonds of **E***·$(H_2O)_3$ computed as the energy difference between **E***·$(H_2O)_3$ and the $(H_2O)_3$ chain is more negative by 12 kcal/mol than that for **E***·$(H_2O)_2$[18] (Table 1S). This result further illustrates the strengthening of the H-bond in the water-wire cluster.

The longer O_1−H_1 and $C_5{=}O_5$ bond lengths and the shorter $H_1 \cdots O_{2w1}$ and $H_{4w3} \cdots O_5$ distances in the **E***·$(H_2O)_3$ complex as compared to those of the open **E***·$(H_2O)_2$[18] and the **E***·$(H_2O)_4$[18] clusters suggest cooperative effects that reinforce the proton acceptor and proton donor properties of the solvent molecules, Table 1S. These cooperative effects are also present in the ground state but are larger in the excited state. On the other side, in our previous study we found that the H-bonded O_1−H_1 group of 7H4MC produced an increase of the carbonyl O_5 basicity, whereas the H-bonded carbonyl O_5 caused a stronger proton donor ability of the OH group.[63] Therefore, a cooperative effect along the entire H_1−O_1−$C_1 \cdots C_5$−O_5 chain of the coumarin ring (Figure 1) is observed also when its donor and acceptor groups are H-bonded with the solvent molecules.

The survey of the structural and energetic data reveals that, among the clusters studied in the S_0 state, the water-wire enol cluster offers the largest acidity and basicity of 7H4MC, which increases further in the first excited state. Moreover, by excitation to the $\pi\pi^*$ state and during the PT process the hydrogen bonds are strengthened in relation to the ground state and assist the PT through the H-bonded water wire. The incipient proton transfer manifests itself via structural changes at the proton injection site at the O_1−H_1 group of **E**·$(H_2O)_3$, since the calculated O_1−H_1 bond length greatly elongates in the S_1 state relative to the isolated **E** molecule. Also, the calculated enol−$O_1 \cdots O_2$ distance in S_1, 2.66 Å (2.64 Å in C_1 symmetry), is close to the typical $O \cdots O$ distances in proton-transfer systems, e.g., 2.55 Å, calculated for the $H_9O_4^+$ cation.[64] For comparison, the larger $O \cdots O$ distance (2.72 Å) for 7HQ·$(H_2O)_3$ in the excited state, calculated at the CIS/6-31G(d,p) level, did not support the PT along the water wire.[64]

III.D. Potential Energy Profile of the Excited-State Proton Transfer. In Figure 2 we present the minimum-energy path profiles along the PT reaction coordinate in the lowest excited state calculated at various computational levels. The coordinate-driven reaction path approach has been used for the description of the proton transfer as it was described in Computational Procedures. Points 1−6 of the PT coordinate (Figure 2) correspond to the optimized structures with fixed and consecutively increased O_1−H_1 distances (stepwise by 0.1 Å starting from the enol form, point 1, R_{O1H1} = 1.000 Å). Starting with the approximate saddle point (point no. 7, R_{O1H1} = 1.696 Å) of the PE curve a spontaneous, barrierless proton-transfer process during the geometry optimization is observed leading to the keto form. The points of the PT coordinate after the saddle point correspond to selected structures of the geometry optimization process of the spontaneous PT. Corresponding Cartesian coordinates are collected in the Supporting Information. The selection of these points is to some extent arbitrary. Our main point was to show the existence of the just-mentioned barrierless path. It is clear that even more favorable reaction paths will exist. Corresponding intra- and intermolecular OH bond distances computed at the TDDFT/SVPD level are depicted in Figure 3. In the first step, the PT was computed on the S_1 surface under C_s symmetry restriction for a planar arrangement of the water molecules. The increase of the O_1−H_1 distance leads to a concomitant decrease of the H_1−O_2 distance and to an increase
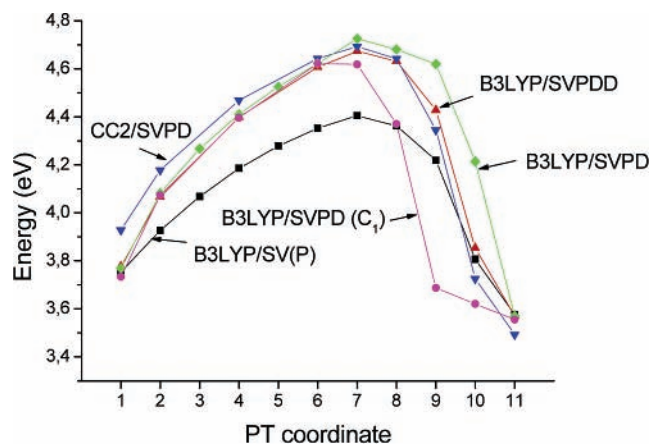
Figure 2. PE profiles of the ESPT reaction path $\mathbf{E}^* \rightarrow \mathbf{K}^*$ of 7H4MC along the water wire in the $S_1{}^1(\pi\pi^*)$ state calculated at different levels of theory. Energies are given relative to the ground-state energy minimum of the respective method. Points 1–6 of the PT coordinate correspond to the optimized structures with fixed and consecutively increased O_1–H_1 distances (stepwise by 0.1 Å starting from the enol form, point 1, $R_{O1H1} = 1.000$ Å). Points 7–10 correspond to selected structures of the optimization of the spontaneous PT process starting at point 7. Point 11 is the keto form.
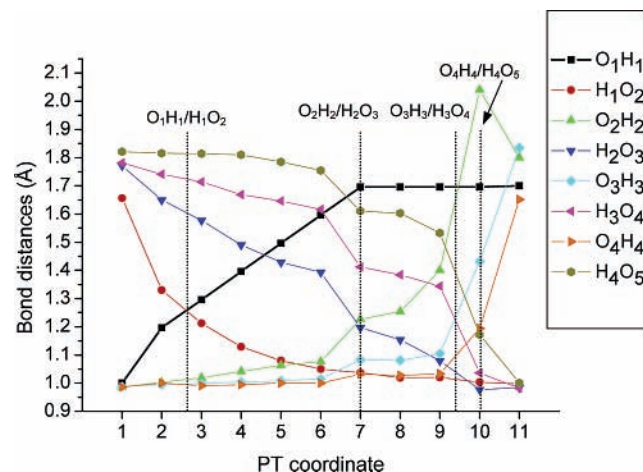
Figure 3. OH bond distances along the $(H_2O)_3$ water chain optimized at the TDDFT/SVPD level for the $S_1{}^1(\pi\pi^*)$ state. Broken vertical lines indicate the positions of proton transfer by the points where the migrating proton is in the middle between its two oxygen atoms. For atom numbering see Figure 1.

of the S_1 energy. At the same time, the hydrogen bond distances H_2–O_3 and H_3–O_4 decrease, leading to an overall contraction of the water chain at the very beginning of the PT. At point 7 (O_1–$H_1 = 1.696$ Å) the (approximate) saddle point is reached. Continuing with successive optimization steps at this point, spontaneous PT occurred leading finally to the $\mathbf{K}^*\cdot(H_2O)_3$ form. Points 8–11 were selected from the geometry optimization procedure in order to represent the remaining geometry changes of the spontaneous PT. The positions of the proton transfer are indicated in Figure 3 by broken vertical lines at positions where the migrating proton is in the middle between its two oxygen atoms. The figure shows that the proton transfer is performed in subsequent steps in a tightly coupled system of $O\cdots H\cdots O$ bonds. The SV(P) basis gave similar results. Calculations with larger basis sets and also with the RI-CC2 method were performed using the SV(P) and SVPD reaction-path geometries. In Table 3 corresponding energy barriers, E_b, are collected using point 7 as the approximate transition-state structure. It should be noted that the ground-state energy curve was always located significantly below the S_1 curve and S_0/S_1 crossing did not occur.

TABLE 3: Energy Barriers (E_b, kcal/mol) of the ESPT Reaction of 7H4MC·$(H_2O)_3$ in the S_1 State Calculated with Respect to the Corresponding S_1 enol Minimum

geometry	method	symmetry	E_b
TDDFT/SV(P)	TDDFT/SV(P)	C_s	15.0
TDDFT/SV(P)	TDDFT/SV(P)	C_1	17.2
TDDFT/SV(P)	TDDFT/SVPD	C_s	20.7
TDDFT/SV(P)	TDDFT/SVPD	C_1	20.5
TDDFT/SV(P)	TDDFT/SVPDD	C_s	20.7
TDDFT/SVPD	TDDFT/SVPD	C_s	22.1
TDDFT/SV(P)	CC2/SV(P)	C_s	12.0
TDDFT/SV(P)	CC2/SVPD	C_s	17.7
TDDFT/SV(P)	CIS/SVPD	C_s	39.7

Inspection of Table 3 shows a barrier of 15.0 kcal/mol at the TDDFT/SV(P) level and of 20.7 kcal/mol at the TDDFT/SVPD level (in C_s symmetry). Extension of the basis set by additional diffuse functions does not change the energy barrier further. The CIS barrier height is obviously overestimated (39.7 kcal/mol). This finding is in line with previous experience reported in the literature.[11,45] Both CC2 and TDDFT methods give energy barriers quite close to each other (difference ~3 kcal/mol).

The TDDFT energy profile of the PT reaction was calculated also without symmetry restriction using the SV(P) and SVPD basis sets. The nonbonded H atoms of the water molecules were moved out-of-plane in the cis position. The out-of-plane distortion of the non-H-bonded H(O2) and H(O4) atoms was performed into the same direction (above the plane) and the H(O3) atom was moved below the plane. Among the other possible rotamers, this cis-rotamer was found to be the most stable one in 7HQ·$(H_2O)_3$.[64] The O atoms of the water molecules are also located out-of-plane of the coumarin ring. It is worth noting that the structure at the PE barrier shows a shorter O_1–H_1 bond length (1.596 Å) in C_1 symmetry than that in C_s symmetry path ($R(O_1$–$H_1) = 1.696$ Å). The barrier height in C_1 symmetry is slightly changed (up to 2 kcal/mol) with respect to the one obtained in C_s, symmetry (see Table 3). The complete Cartesian geometries of $\mathbf{E}^*\cdot(H_2O)_3$, TS*, and $\mathbf{K}^*\cdot(H_2O)_3$ structures at the TDDFT/SVPD level in C_s and C_1 symmetries are given in the Supporting Information.

To characterize the nature of the lowest S_1 state and of the other low-lying excited states along the reaction path, PE profiles of the PT curves have been computed for the $2^1A'$, $3^1A'$, $1^1A''$, and $2^1A''$ excited states at the TDDFT/SVPDD level with the S_1 optimized structures computed at the TDDFT/SV(P) level (see Figure 4). For comparison, the PE curve of the ground state, calculated at the S_1-optimized geometry, is also included in this figure. The molecular orbitals (MOs), which take part in the electronic excitations of the enol and keto minima as well as of the transition state, are presented in Figure 5. The 50a′ orbital is a lone pair orbital located at the carbonyl moiety. The 11a″ orbital is the highest occupied MO (HOMO) and 12a″ is the lowest unoccupied MO (LUMO). The 10a″ orbital participates in the electronic excitation to the second $\pi\pi^*$ state. MO 51a′ is a diffuse (Rydberg-type) orbital located on one of the water molecules. The different electronic states considered here are characterized in Table 4 by the dominant orbital excitation. TDDFT and RI-CC2 results agree qualitatively very well. At the enol side, the first excited state is the $2^1A'(\pi\pi^*)$ state, followed by the $3^1A'(\pi\pi^*)$, $1^1A''(n\pi^*)$, and $2^1A''(\pi\sigma^*)$ states. On extension of the O_1–H_1 bond the $\pi\sigma^*$ state is stabilized, crosses with the $n\pi^*$ state, and thus becomes the second excited state (see Figure 4). Similar $\pi\sigma^*$ stabilization was found by Domcke and Sobolowoski[65] for the phenol–ammonia complex and by Tanner et al. for 7HQ·$(NH_3)_3$.[10] However, the $\pi\sigma^*$ state of 7H4MC·$(H_2O)_3$ does not cross the
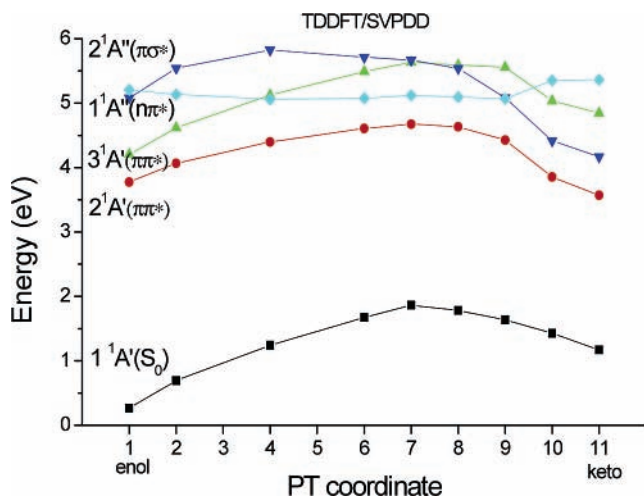
Figure 4. Proton-transfer curves for S_0 and low-lying excited states of 7H4MC·$(H_2O)_3$, calculated at the TDDFT/SVPDD level with S_1-optimized structures using the TDDFT/SV(P) approach. Energies are given relative to the ground-state energy minimum.

TABLE 4: Characterization of the Lowest Electronic States by Orbital Excitation

state	orbital excitation	weight (%) TDDFT/CC2
	E·$(H_2O)_3$	
$2^1A(\pi\pi^*)$	11a−12a	91/87
$3^1A(\pi\pi^*)$	10a−12a	91/77
$1^1A(n\pi^*)$	50a−12a	96/78
$2^1A(\pi\sigma^*)$	11a−51a	96/72
	transition state (point 7)	
$2^1A(\pi\pi^*)$	11a−12a	94/85
$1^1A(\pi\sigma^*)$	11a−51a	99/61
$3^1A(\pi\pi^*)$	10a−12a	93/77
$2^1A(n\pi^*)$	50a−12a	98/96
	K·$(H_2O)_3$	
$2^1A(\pi\pi^*)$	11a−12a	93/91
$1^1A(n\pi^*)$	50a−12a	99/96
$3^1A(\pi\pi^*)$	10a−12a	91/89
$2^1A(\pi\sigma^*)$	11a−51a	97/69

$2^1A'(\pi\pi^*)$ state. The calculations show that the latter state remains the lowest excited state throughout the PT reaction path. The same trend was observed also for the C_1 reaction path; see Figure 1S in the Supporting Information. Obviously, the reaction mechanism here is completely different from the one observed in the NH_3 wire of 7HQ·$(NH_3)_3$.[10] The PE curve of the $\pi\sigma^*$ state shows two shallow minima: the first one corresponds to a structure with the transferred hydrogen atom on the first H-bonded water molecule: the second one, with hydrogen atom bound to the second water molecule.

To illustrate the consequences of the just-described orbital occupations, in Figure 6 the electron density difference between the ground and lowest $\pi\pi^*$ state is depicted for the saddle-point structure. The first observation is that this difference is located almost exclusively in the region of 7H4MC. The electron density increases on the proton acceptor site (O_5) and decreases on the O_1 of the proton donor group, indicating an increase of the O_5(=C) basicity and a weakening of the O_1−H_1 bond. These density changes facilitate the ES enol-to-keto reaction. Moreover, we can conclude that the shift of electron density within the organic chromophore 7H4MC due to the optical excitation is the driving force for the ESPT.

Natural population analyses of all 7H4MC·$(H_2O)_3$ structures along the reaction path have been performed for the ground

state and the first excited state at the CIS/SVP level. Most important for the question of proton vs hydrogen atom transfer is the charge of the H_2 and H_3 atoms in the approximate transition state (point 7). They carry a natural charge of $0.61e$ each, revealing that the $\pi\pi^*$ state reaction of 7H4MC involves a proton transfer and not a H atom transfer. The charge separation leads to long-range polarization effects, which have already been observed above in the form of the strongly coupled geometry changes in the water chain. The results obtained are in line with the dominant $\pi\pi^*$ character of the S_1 state throughout the reaction path. This finding is in agreement with the population analysis performed by Tanner et al.[10] on 7HQ·$(NH_3)_3$, where for the higher excited $\pi\pi^*$ state a charge of $0.70e$ for the NH_4 moiety had been found, in opposition to $-0.41e$ found for the $\pi\sigma^*$ state.

The just-described charge separation is also reflected in the change of the dipole moment. The water chain is approximately oriented along the z coordinate axis (see Figure 6). The total dipole moment and z-component μ_z of the dipole moment are collected in Table 3S of the Supporting Information. In the course of the PT the total dipole moment and μ_z (in absolute value) strongly increase in the S_1 state up to the approximate transition state and then decrease to the values of the keto structure. The increase of the dipole moment correlates well with the charge separation due to the proton-transfer mechanism described in the previous paragraph. The decrease of the dipole moment from the transition state to the keto form indicates increasing charge transfer, which could be considered as a driving force for the spontaneous ESPT reaction. It should be noted that the isolated enol 7H4MC and keto 7H4MC forms show opposite direction of the dipole moments in the z-direction and also support the charge transfer going from enol to keto.

To check the TDDFT potential energy curves, RI-CC2/SVPD calculations have been performed also. Corresponding proton-transfer curves, computed for four excited states, are presented in Figure 7a. The calculated CC2 curves for the $\pi\pi^*$ and $n\pi^*$ states show a behavior similar to that for the curves obtained with the TDDFT method (Figure 4). As an important observation, we find that the PE curve for the $\pi\sigma^*$ state is flatter and even more distant to the lowest $\pi\pi^*$ state as compared to the TDDFT case. Therefore, both RI-CC2 and TDDFT methods are in good agreement: the ESPT occurs on the S_1 surface, characterized throughout as $\pi\pi^*$ state, and no crossing with the $\pi\sigma^*$ state is found.

CIS/6-31G(+)G(d,p) calculations of the S_1 enol → keto tautomerization in the 7HQ·$(NH_3)_3$ system showed a crossing between the lowest $\pi\pi^*$ and $\pi\sigma^*$ states.[10] For the sake of comparison we performed CIS/SVPD calculations for the 7H4MC·$(H_2O)_3$ cluster. The results are displayed in Figure 7b. The calculations confirmed the $\pi\pi^*$ state as the lowest excited state throughout the ESPT reaction path. No crossing between the $\pi\pi^*$ and the $\pi\sigma^*$ states was found. On the other hand, the CIS/SVPD calculations predict that both low-lying $^1A''$ states are of $\pi\sigma^*$ character throughout the reaction path. This result is at variance with the observed stabilization of the $n\pi^*$ state found with the TDDFT and CC2 methods on the keto side of the PT reaction (compare Figure 7b with Figure 4 and Figure 7a). The CIS method predicts that the lowest state along the ESPT is the $\pi\pi^*$ state in agreement with CC2 and TDDFT results. However, all excited-state curves are shifted by 1−2 eV to higher energies as compared to the RI-CC2 and TDDFT curves. Moreover, as it has already been discussed in connection with Table 3, the CIS energy barrier of S_1 is significantly overestimated and the reaction is endoergic (Table 1).

ESPT in 7H4MC along a Hydrogen-Bonded Water Wire

J. Phys. Chem. A, Vol. 111, No. 1, 2007 **133**
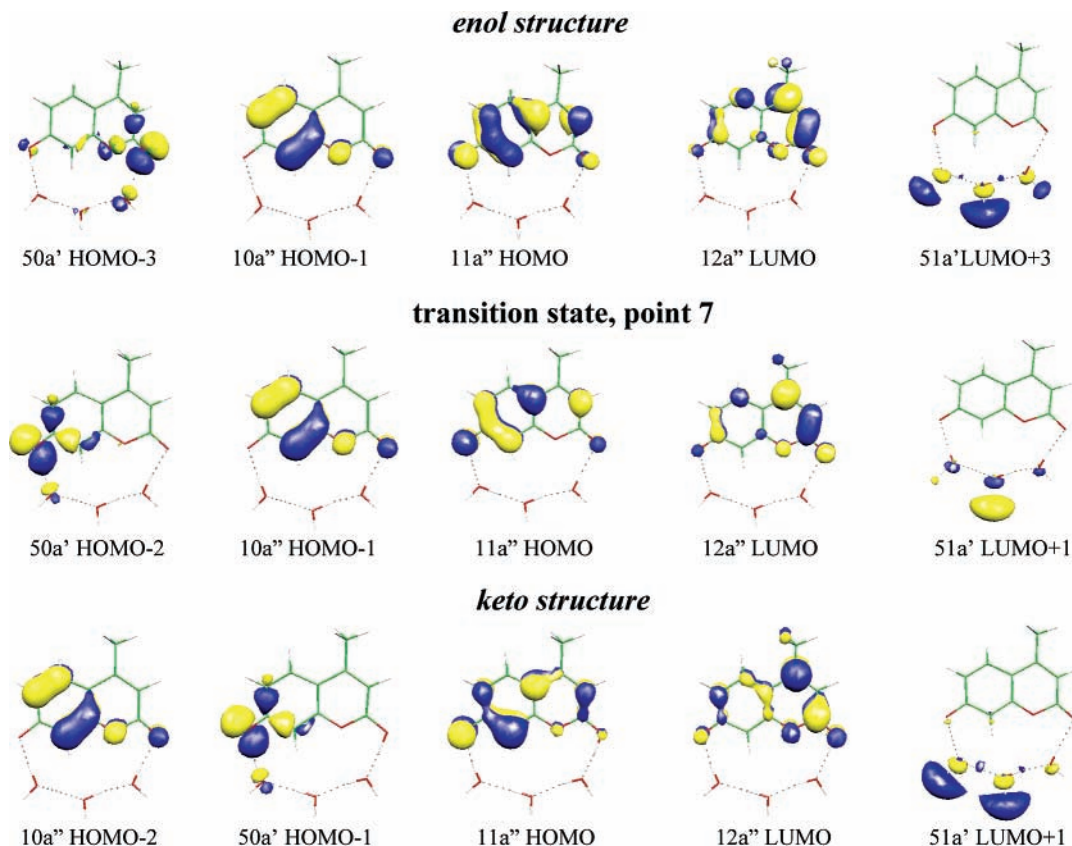
Figure 5. Evolution of occupied and unoccupied molecular orbitals that contribute dominantly to the $1^1(\pi\pi^*)$, $2^1(\pi\pi^*)$, $^1(n\pi^*)$, and $^1(\pi\sigma^*)$ transitions for the enol, transition state (point 7), and keto structures along the water wire (cutoff value 0.05).
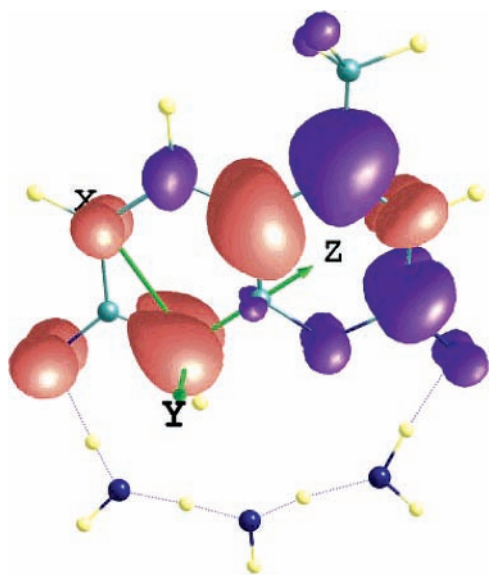

Figure 6. Electron difference density between the $\pi\pi^*$ and the ground state at the TS structure (point 7) of 7H4MC·(H$_2$O)$_3$, calculated with the CIS/SVP method. The black (or dark blue) regions indicate an increase of electron density and the gray (or red) regions a decrease of electron density.

Preliminary TDDFT investigations on the 7HQ·(NH$_3$)$_3$ system using the TDDFT/SVPD method led to a crossing of the $\pi\pi^*$ and $\pi\sigma^*$ states and to a hydrogen atom transfer mechanism as reported by Tanner et al.[10] Thus, the different transfer mechanisms (proton transfer in the S$_1$ state of 7H4MC·(H$_2$O)$_3$ and hydrogen atom transfer in S$_1$ state of 7HQ·(NH$_3$)$_3$) are due to the different system properties and are not artifacts of the computational methods used.

IV. Conclusions

The nondissociative ESPT in 7H4MC has been modeled by a "wire" of three hydrogen-bonded water molecules connecting the proton donor (H−O) and the proton acceptor (=O) sites. In agreement with the fluorescence evidence for the existence of an excited-state keto form of 7H4MC, TDDFT and RI-CC2 calculations in gas phase and solution predicted a lower energy of the **K*** structure in comparison to **E***, pointing to the energetic possibility of enol*-to-keto* proton transfer. The TDDFT and CC2 methods appear to be reliable approaches for description of the energy surfaces for ESPT of 7H4MC along a water wire. The S$_1$ state along the reaction path of the ESPT has $\pi\pi^*$ character. No intersections with other low-lying states, in particular with the $\pi\sigma^*$ state, were observed. The S$_1$ potential energy curve shows minima (under C_s symmetry restriction) of *enol-* and *keto-*7H4MC·(H$_2$O)$_3$ structures, separated by a barrier of 17−20 kcal/mol. Relaxation of the C_s symmetry constraint has only a small effect on the computed barrier height. The transition state on the PE curve is characterized by a highly correlated structure where the first proton is completely transferred from the enol OH to the first water molecule, the proton of the first water is close to the midpoint to the next water molecule, and the OH bond of the second water is strongly stretched. During the following optimization steps, spontaneous PT occurs and the final structure is the **K***·(H$_2$O)$_3$ form.

The observed structural reorganization in the water-wire cluster is classified as proton transfer based on the fact that the lowest excited singlet state has $\pi\pi^*$ character and on population analysis. By excitation to the $\pi\pi^*$ state and during the PT process the hydrogen bonds are strengthened in relation to the ground state and assist the PT through the H-bonded solvent wire. The structural and energetic results for **E***·(H$_2$O)$_3$ suggest cooperative effects that reinforce the proton acceptor and proton
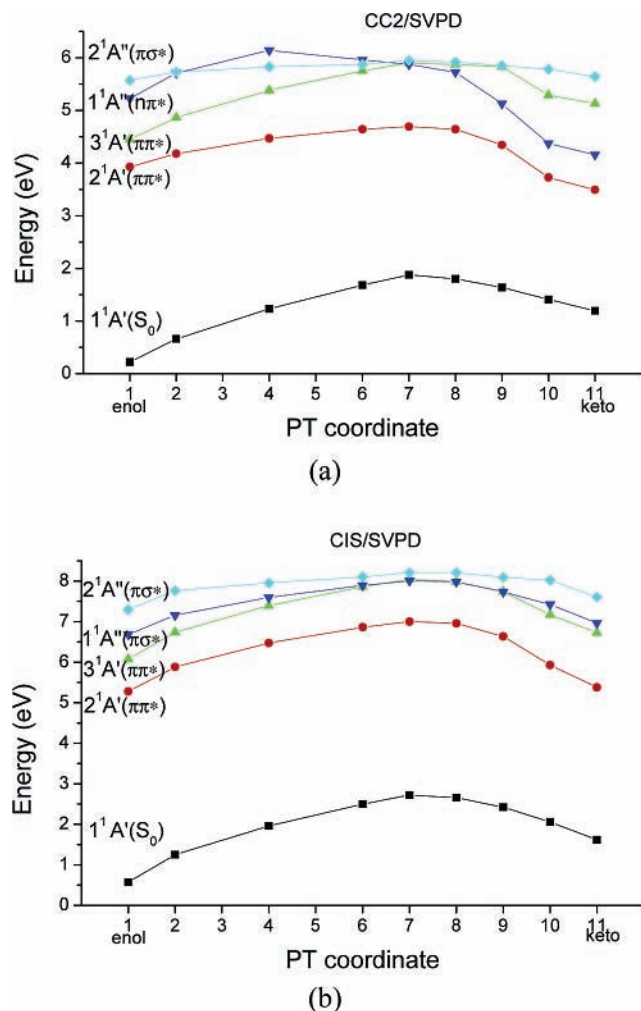
Figure 7. Proton-transfer curves for S_0 and low-lying excited states of 7H4MC·$(H_2O)_3$, calculated (a) with the CC2/SVPD method and (b) with the CIS/SVPD method at TDDFT/SV(P) S_1-optimized structures. Energies are given relative to the ground-state energy minimum.

donor properties of 7H4MC. In the $\pi\pi^*$ state the electron density increases on the proton acceptor site (O_5) and decreases on the O_1 of the proton donor group, and thus, the shift of electron density within the organic chromophore 7H4MC due to optical excitation appears to be the driving force for the reaction of ESPT. The spontaneous ESPT reaction is supposed to be driven by long-range polarization effects.

The $\pi\sigma^*$ state has been identified in our calculations as a higher excited state. In the vertical excitation at the enol side it has been computed as the fourth excited state. It is stabilized by the stretching of the enol OH bond. However, this stabilization is not sufficient to achieve crossing with the lowest $\pi\pi^*$ state. This qualitative behavior has been confirmed by TDDFT, RI-CC2, and CIS methods. Thus, the ESPT reaction path of 7H4MC·$(H_2O)_3$ is found to be qualitatively different from that of 7HQ·$(NH_3)_3$.[10] In the latter case, a crossing of the $\pi\pi^*$ and $\pi\sigma^*$ states and three local minima with the migrating hydrogen atom localized on each of the ammonia molecules were found. Preliminary calculations performed by us using the TDDFT/SVPD approach confirmed the $\pi\pi^*$ and $\pi\sigma^*$ crossing reported in ref 10. Thus, we conclude that this difference is not due to the use of different computational methods but is due to difference in the inherent properties of the molecular systems. It should be mentioned that in the three-water-wire cluster of 7HQ the tautomerization and PT reaction have not been observed, showing that the chain type is important for the PT

reaction in 7HQ clusters.[10,64] The present study revealed that the type of the proton acceptor sites, N or O, might also play an important role for the PT process.

The most extended calculation (RI-CC2/SVPD) gives an energy barrier of 17.7 kcal/mol. This is substantially larger than the 10.8 kcal/mol for the first barrier reported in ref 10. The present calculations on the proton-transfer mechanism were carried out for the isolated system. It can be expected that the ionic mechanism of PT in 7H4MC·$(H_2O)_3$ will be stabilized in polar solvents and the energy barrier could be reduced substantially, making the ESPT more favorable. Extended investigations will be necessary using, e.g., larger cluster models in order to obtain more information on solvation effects on the PT barrier in the excited state.

Supporting Information Available: Tables 1S–3S and Figure 1S, showing proton-transfer curves of S_0 and low-lying excited states for 7H4MC·$(H_2O)_3$ calculated with the TDDFT/SVPD (C_1 symmetry) approach, and Cartesian geometries and total energies of the structures corresponding to points 1–11 of the PT coordinate computed at the TDDFT/SVPD level in C_s symmetry and of $\mathbf{E}^*(H_2O)_3$, TS, and $\mathbf{K}^*(H_2O)_3$ forms in C_1 symmetry. This material is available free of charge via the Internet at http://pubs.acs.org.are presented in.

References and Notes

(1) Balamurali, M. M.; Dogra, S. K. *Chem. Phys.* **2004**, *305*, 95, and references therein.

(2) Ingham, K. C.; Abu-Elgheit, M.; El-Bayoumi, M. A. *J. Am. Chem. Soc.* **1971**, *93*, 5023.

(3) Bardez, E.; Chatelain, A.; Larrey, B.; Valeur, B. *J. Phys. Chem.* **1994**, *98*, 2357.

(4) Bardez, E.; Boutin, P.; Valeur, B. *Chem. Phys. Lett.* **1992**, *191*, 142.

(5) Lee, S. I.; Jang, D. J. *J. Phys. Chem.* **1995**, *99*, 7537.

(6) Kim, T. G.; Lee, S. I.; Jang, D.; Kim, Y. *J. Phys. Chem.* **1995**, *99*, 12698.

(7) Itoh, M.; Adachi, T.; Tokumura, K. *J. Am. Chem. Soc.* **1984**, *106*, 850.

(8) Nakagawa, T.; Kohtani, S.; Itoh, M. *J. Am. Chem. Soc.* **1995**, *117*, 7952.

(9) Li, Q.-S.; Fang, W.-H. *Chem. Phys. Lett.* **2003**, *367*, 637.

(10) (a) Tanner, C.; Manca, C.; Leutwyler, S. *Science* **2003**, *302*, 1736. (b) Tanner, C.; Manca, C.; Leutwyler, S. *J. Chem. Phys.* **2005**, *122*, 204326. (c) Manca, C.; Tanner, C.; Leutwyler, S. *Int. Rev. Phys. Chem.* **2005**, *24*, 1.

(11) Seixas de Melo, J. S.; Becker, R. S.; Macanita, A. L. *J. Phys. Chem.* **1994**, *98*, 6054.

(12) Pavlopoulos; T. G. *IEEE J. Quantum Electron.* **1973**, *9* (5), 510.

(13) Zinsli, P. E. *J. Photochem.* **1974/75**, *3*, 55.

(14) Schulman, S. G.; Rosenberg, L. *J. Phys. Chem.* **1979**, *83* (4), 447.

(15) Moriya, T. *Bull. Chem. Soc. Jpn.* **1983**, *56*, 6.

(16) Moriya, T. *Bull. Chem. Soc. Jpn.* **1988**, *61*, 1873.

(17) (a) Seixas de Melo, J.; Fernandes, P. F. *J. Mol. Struct.* **2001**, *565–566*, 69. (b) McCarthy, P. K.; Blanchard, G. J. *J. Phys. Chem.* **1993**, *97*, 12205.

(18) Georgieva, I.; Trendafilova, N.; Aquino, A. J. A.; Lischka, H. *J. Phys. Chem. A* **2005**, *109*, 11860.

(19) Jones, G., II; Jimenez, J. A. C. *J. Photochem. Photobiol., B* **2001**, *65*, 5.

ESPT in 7H4MC along a Hydrogen-Bonded Water Wire

J. Phys. Chem. A, Vol. 111, No. 1, 2007 **135**

(20) Nielsen, B. E. Coumarins Patterns in the Umbrelliferae. In *The Biology and Chemistry of the Umbrelliferae*; Heywood, V. H., Ed.; Academic Press: London, 1971; p 325.

(21) Kam, C. M.; Kerrigan, J. E.; Plaskon, R. R.; Duffy, E. J.; Lollar, P.; Suddath, F. L.; Powers, J. C. *J. Med. Chem.* **1994**, *37*, 1298.

(22) Yamada, Y.; Okamoto, M.; Kikuzaki, H.; Nakatani, N. *Biosci. Biotechnol. Biochem.* **1997**, *61*, 740.

(23) (a) Rosskopt, F.; Kraus, J.; Franz, G. *Pharmazie* **1992**, *47*, 139. (b) McCulloch, P.; George, W. D. *Br. J. Cancer* **1989**, *59*, 179.

(24) Lazarova, G.; Kostova, I.; Neychev, H. *Fitoterapia* **1993**, *64*, 134.

(25) Matolcsy, G.; Nadasy, M.; Andriska, V. *Pesticide Chemistry*; Studies in Environmental Science; Elsevier: Budapest, 1988; p *32*.

(26) Nakashima, M.; Sousa, J. A.; Clapp, R. C. *Nat. Phys. Sci.* **1972**, *235*, 16.

(27) Abdel-Mottaleb, M. S. A.; El-Sayed, B. A.; Abo-Aly, M. M.; El-Kady, M. Y. *J. Photochem. Photobiol., A* **1989**, *46*, 379.

(28) Balter, A.; Rolinski, O. *Z. Naturforsh.* **1984**, *39A*, 1035.

(29) Manca, C.; Tanner, C.; Coussan, S.; Bach, A. *J. Chem. Phys.* **2004**, *121*, 2578.

(30) Lahmani, F.; Douhal, A.; Breheret, E.; Zehnacker-Rentien, A. *Chem. Phys. Lett.* **1994**, *220*, 235.

(31) Bach, A.; Leutwyler, S. *Chem. Phys. Lett.* **1999**, *299*, 381.

(32) Bach, A.; Coussan, S.; Müller, A.; Leutwyler, S. *J. Chem. Phys.* **2000**, *112*, 1192.

(33) Bach, A.; Leutwyler, S. *J. Chem. Phys.* **2000**, *112*, 560.

(34) Coussan, S.; Bach, A.; Leutwyler, S. *J. Phys. Chem. A* **2000**, *104*, 9864.

(35) Coussan, S.; Meuwly, M.; Leutwyler, S. *J. Chem. Phys.* **2001**, *114*, 3524.

(36) Bach, A.; Tanner, C.; Manca, C.; Frey, H.-M.; Leutwyler, S. *J. Chem. Phys.* **2003**, *119*, 5933.

(37) Coussan, S.; Manca, C.; Tanner, C.; Bach, A.; Leutwyler, S. *J. Chem. Phys.* **2003**, *119*, 3774.

(38) Sobolewski, A. L.; Domcke, W. *J. Phys. Chem. A* **1999**, *103*, 4494.

(39) Sobolewski, A. L.; Domcke, W. *Chem. Phys.* **2000**, *259*, 181.

(40) Sobolewski, A. L.; Domcke, W. *J. Phys. Chem. A* **2001**, *105*, 9275.

(41) Sobolewski, A. L.; Domcke, W.; Dedonder-Lardeux, C.; Jouvet, C. *Phys. Chem. Chem. Phys.* **2002**, *4*, 1093.

(42) Furche, F.; Ahlrichs, R. *J. Chem. Phys.* **2002**, *117*, 7433.

(43) Bauernschmitt, R.; Ahlrichs, R. *Chem. Phys. Lett.* **1996**, *256*, 454.

(44) Bauernschmitt, R.; Häser, M.; Treutler, O.; Ahlrichs, R. *Chem. Phys. Lett.* **1997**, *264*, 573.

(45) Sobolewski A. L.; Domcke W. *Phys. Chem. Chem. Phys.* **1999**, *1*, 3065.

(46) Christiansen, O.; Koch, H.; Jørgensen, P. *Chem. Phys. Lett.* **1995**, *243*, 409.

(47) Hättig, C. *J. Chem. Phys.* **2003**, *118*, 7751.

(48) Aquino, A. J. A.; Lischka, H.; Hättig C. *J. Phys. Chem. A* **2005**, *109*, 3201.

(49) Ahlrichs, R.; Bär, M.; Häser, M.; Horn, H.; Kölmel, C. *Chem. Phys. Lett.* **1989**, *162*, 165.

(50) Köhn, A.; Hättig, C. *J. Chem. Phys.* **2003**, *119*, 5021.

(51) Becke, A. D. *J. Chem. Phys.* **1993**, *98*, 5648.

(52) Weigend, F.; Häser, M.; Patzelt, H.; Ahlrich, R. *Chem. Phys. Lett.* **1998**, *294*, 143.

(53) Schäfer, A.; Horn, H.; Ahlrichs, R. *J. Chem. Phys.* **1992**, *97*, 2571.

(54) Boys, S. F.; Bernardi, F. *Mol. Phys.* **1970**, *19*, 553.

(55) van Duijneveldt, F. B.; van Duijneveldt-van de Rijdt, J. G. C. M.; van Lenthe, J. H. *Chem. Rev.* **1994**, *94*, 1873.

(56) Valiron, P.; Mayer, I. *Chem. Phys. Lett.* **1997**, *275*, 46.

(57) Xantheas, S. S. *J. Chem. Phys.* **1996**, *104*, 8821.

(58) Miertus, S.; Scrocco, E.; Tomasi, J. *Chem. Phys.* **1981**, *55*, 117.

(59) Miertus, S.; Tomasi, J. *Chem. Phys.* **1982**, *65*, 239.

(60) Cossi, M.; Barone, V.; Cammi, R.; Tomasi, J. *Chem. Phys. Lett.* **1996**, *255*, 327.

(61) *Gaussian 03*, Revision C.02. References cited in www.gaussian-.com.

(62) (a) Read, A. E.; Curtiss, L. A.; Weinhold, F. *Chem. Rev.* **1988**, *88*, 899. (b) Carpenter, J. E.; Weinhold, F. *J. Mol. Struct. (THEOCHEM)* **1988**, *169*, 41.

(63) Georgieva, I.; Mihaylov, Tz.; Bauer, G.; Trendafilova, N. *Chem. Phys.* **2004**, *300*, 119.

(64) Bach, A.; Coussan, S.; Müller, A.; Leutwyler, S. *J. Chem. Phys.* **2000**, *113*, 9032.

(65) Domcke, W.; Sobolewski, A. L. *Science* **2003**, *302*, 1693.